ELSEVIER

Marine Geology 168 (2000) 25–44

MARINE GEOLOGY
INTERNATIONAL JOURNAL OF MARINE GEOLOGY, GEOCHEMISTRY AND GEOPHYSICS

www.elsevier.nl/locate/margeo

The Late Weichselian glaciation of the Franz Victoria Trough, northern Barents Sea: ice sheet extent and timing

H.P. Kleiber, J. Knies*, F. Niessen

Alfred Wegener Institute for Polar and Marine Research, Columbusstrasse, Postfach 120161, D-27515 Bremerhaven, Germany

Received 13 October 1999; accepted 2 May 2000

Abstract

High resolution seismic profiles (PARASOUND, 4 kHz) and three sediment cores from the Franz Victoria Trough and the adjacent continental slope were studied in order to constrain the timing and extent of the northern Svalbard/Barents Sea ice sheet during the Late Weichselian glaciation. Stacked debris flow lobes and layers of glacimarine diamicton on the lower continental slope indicate that large quantities of glacially derived sediments were deposited by the northern Svalbard/Barents Sea ice sheet directly onto the upper continental slope at approximately 23 ^{14}C ka. A grounding-line advance to the shelf break is supported by the identification of diamicton, interpreted as till, in the seismic profile near the shelf break. After several ice sheet instabilities marked by significant input of ice rafted detritus to the continental margin, the disintegration of the northern Svalbard/Barents Sea ice sheet (Termination Ia) is indicated by a distinct pulse of ice rafted detritus at 15.4 ^{14}C ka and the transition to an isotopically defined meltwater signal. The drastic change in sedimentary pattern on the upper continental slope, dated to about 13.4 ^{14}C ka, is interpreted as grounding-line retreat from the shelf edge. A further stepwise retreat of the northern Svalbard/Barents Sea ice sheet is indicated by pulses of ice rafted detritus which appear to be contemporaneous with the onset of distinct ice rafting events in adjacent areas and pulses of glacimarine sedimentation in the southwestern Barents Sea.

Keywords: Marine geology; Paleoclimate; Barents Sea; Last glacial maximum

1. Introduction

In earlier studies, reconstruction of Late Pleistocene ice sheets along the Eurasian continental margin were discussed controversially, even for the Last Glacial Maximum (LGM) (e.g. Vogt et al., 1994). Postulated scenarios ranged from isolated small ice caps over the Eurasian archipelagos to a large ice sheet covering the entire Siberian shelf and extending far into continental Eurasia (e.g. Hughes et al., 1977; Grosswald, 1980, 1990, 1998; Dunayev and Pavlidis, 1990; Astakhov, 1992, 1998; Elverhøi et al., 1993). For the Barents Sea, the distribution of glacial diamicton and morainal banks leaves little doubt that even the deepest basins were covered by grounded ice during the Late Weichselian (Elverhøi et al., 1990; Solheim et al., 1990; Gataullin et al., 1993; Polyak et al., 1995; Knies et al., 1999, 2000).

Due to severe sea ice conditions, the Franz Victoria Trough (FVT) (Fig. 1) is one of the least accessible and poorly understood areas with respect to the glacial and deglacial history (e.g. Polyak and Solheim, 1994; Forman et al., 1995; Lubinski et al., 1996; Solheim

* Corresponding author. Present address: SINTEF Petroleum Research, Basin Modelling Dept., S.P. Andersen Veg 15, 7465 N-Trondheim, Norway. Fax: + 47 73591102.

E-mail address: jochen.knies@iku.sintef.no (J. Knies).

0025-3227/00/$ - see front matter
PII: S0025-3227(00)00047-5

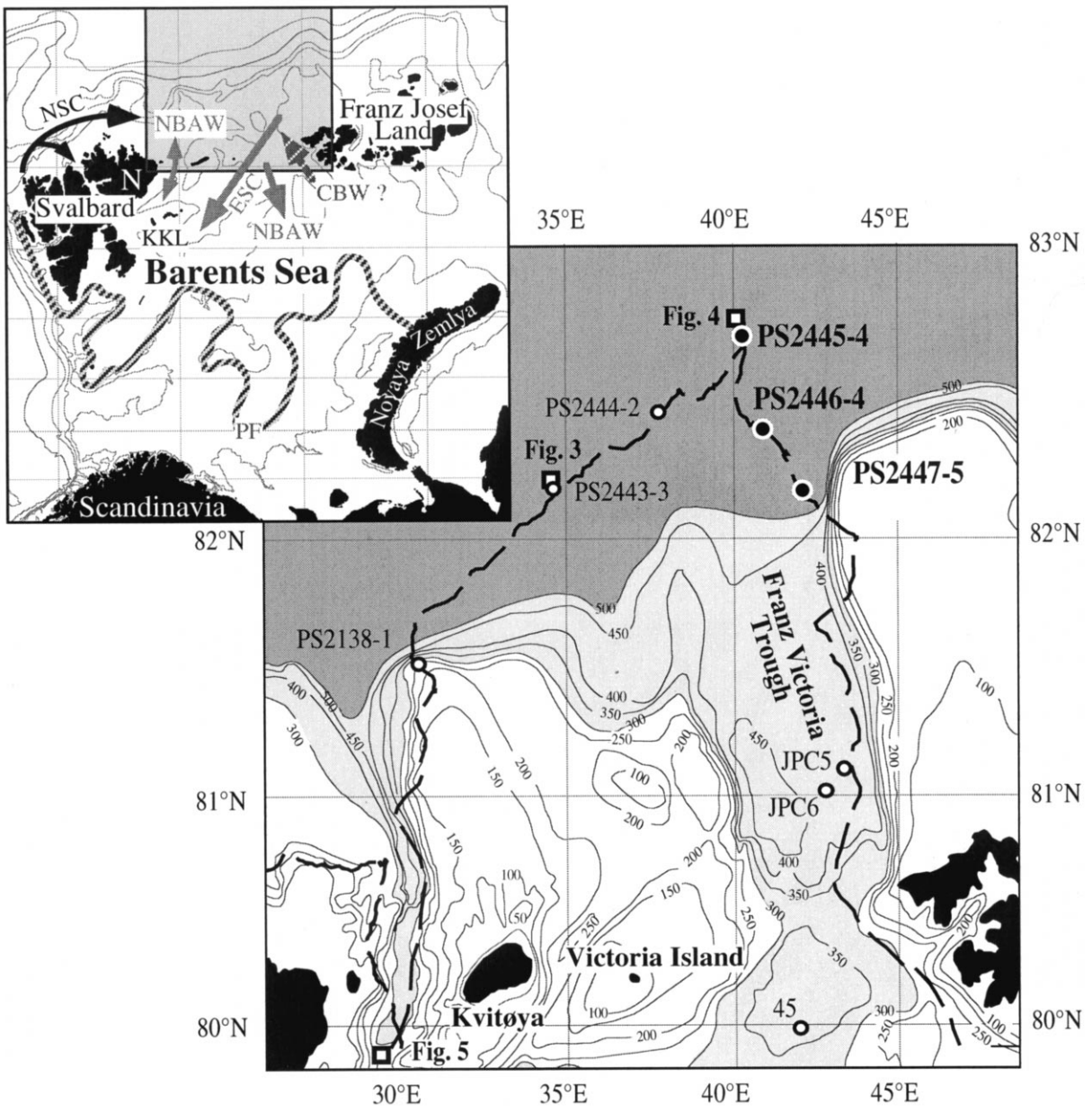

Fig. 1. Regional setting and bathymetry of the study area at the northern Barents Sea continental margin (50 m contours above 500 m). Light gray shading represents water depth greater than 300 m; dark gray shading represents water depth greater than 500 m. The circulation of the main warm surface water currents (Atlantic water: dark arrows), the cold surface currents (Arctic water: light arrows) (modified after Pfirman et al., 1994 and references therein) and the location of the oceanic polar front (PF, striped line) (after Vinje, 1985; Loeng, 1991) are shown. The PF divides colder and fresher Arctic water in the north from relatively warm and saline water of Atlantic origin in the south. N = Nordaustlandet, KKL = Kong Karls Land, NSC = North Spitsbergen Current, ESC = East Spitsbergen Current, NBAW = Northern Barents Atlantic derived Water, CBW = Cold Bottom Water. 45, JPC 5/6 and PS2138 are sites of sediment cores presented by Polyak and Solheim (1994), Lubinski et al. (1996) and Knies and Stein (1998). The investigated ship tracks are shown as black, dotted lines. Open boxes show location of PARASOUND profiles (cf. Figs. 3–5).

and Forsberg, 1996; Landvik et al., 1998). Despite lack of direct evidence, most reconstructions including the recent summary paper by Svendsen et al. (1999 and references therein) suggest that during the Late Weichselian the grounding line of the northern Svalbard/Barents Sea ice sheet (SBIS) reached the outermost, northern margin of the FVT and an initial retreat commenced at ~15 ^{14}C ka. This assumption is based on inferences from the southwestern Barents Sea, the regional uplift pattern, correlations with regional meltwater events, bathymetric features and models of ice sheet dynamics (e.g. Elverhøi et al., 1990, 1993; Lambeck, 1995, 1996; Siegert and Dowdeswell, 1995; Vorren and Laberg, 1997). Recent studies of a 3.5 kHz seismic profile and sediment cores in the southern and the central FVT reveal that the three recorded seismic units represent a typical deglaciation succession of glacial diamicton, interpreted as basal till, overlain by laminated glacimarine and bioturbated postglacial sediments (Polyak and Solheim, 1994; Lubinski et al., 1996). Radiocarbon datings of the laminated glacimarine mud postulate an ice retreat prior to 12.9 and 13.2 ^{14}C ka and suggest that normal marine conditions were established close to 10 ^{14}C ka (Polyak and Solheim, 1994; Lubinski et al., 1996). The 3.5 kHz seismic profile shows that the till bed extends continuously across the central FVT. This implies that the SBIS was grounded down to a modern water depth of at least 470 m (Lubinski et al., 1996). Seismic studies in the northern parts of the trough as far north as 81.5°N also suggest that the sea floor is covered by the same till unit (Landvik et al., 1998; Siegert et al., 1999). However, direct evidence for maximum ice sheet extension and deglaciation patterns from the outer shelf edge do not exist. Therefore, the main objective of this study is to outline a more detailed history of the SBIS in the FVT during the Late Weichselian and provide a more comprehensive framework for future ice sheet modeling along the northern Eurasian continental margin (cf. Landvik et al., 1998). For this reason, we have studied seismic profiles (PARASOUND, 4 kHz) and three sediment cores from the FVT and adjacent continental slope to constrain waxing and waning of the SBIS along the northern Barents Sea margin. The data document spatial and temporal variations in sedimentary environment during the Late Weichselian and provide evidence for the extent of basal till in the FVT.

2. Data acquisition and methods

High resolution sub-bottom profiles were recorded by the hull-mounted PARASOUND echosounder (4 kHz) (cf. Grant and Schreiber, 1990, for technical details). A seismic velocity of 1500 m/s was used to estimate sediment thickness. The evaluated seismic profiles were recorded during RV *Polarstern* cruises ARK-IX/4 (Fütterer, 1994) and ARK-XIII/2 (Niessen and Kleiber, 1997) and are of variable quality. Secondary noise from ice breaking, recording failures due to ice and air bubbles under transmitter/receiver units as well as geometric effects resulting from ice ramming of the vessel caused some sections to be of poor quality. However, successions of high quality profiles, mainly recorded during station time when the vessel drifted with the ice, are sufficient to estimate the extent of the seismic signatures and thus the distribution of the seismic units over the entire continental slope. The different seismic facies are classified after the schemes of Damuth (1975, 1980) and Pratson and Laine (1989).

The investigated sediment cores (PS2445-4, PS2446-4 and PS2447-5) were recovered during the RV *Polarstern* cruises ARK IX/4 (Fütterer, 1994) from the continental margin north of the FVT (Fig. 1), using a gravity (12 cm core diameter) and Kastenlot corer (rectangular cross section of 30×30 cm^2) built at Hydrowerkstätten Kiel, Germany. The sediment cores were routinely sampled at 5–10 cm intervals; additional samples were taken in intervals of changing lithology and/or color. X-ray radiographs were taken continuously downcore from sediment slabs of ca. 1 cm thickness in order to determine clast contents, sedimentological structures, and bioturbation.

Total carbon (TC), total organic carbon (TOC) and nitrogen were determined using a Heraeus CHN-O-RAPID analyzer. Total organic carbon/total nitrogen (C/N) weight ratios characterizing the composition of the organic matter were calculated as total organic carbon/total nitrogen ratios. In general, terrigenous organic matter (TOM) shows C/N-ratios >15, marine organic matter (MOM) C/N-ratios <10 (Scheffer and

Table 1
Results of accelerator mass spectrometry (AMS) ^{14}C performed at the Leibniz Laboratory for Radiometric Dating and Stable Isotope Research, University of Kiel, Germany

Core	Sample number	Depth (cmbsf)	Carbon source	^{14}C-Age (uncorr.)	Error	^{14}C-Age (corr. 440 years)
PS2445-4	KIA4767	131	Mixed forams	14 880	± 130	14 440
PS2445-4	KIA366	191	N. pachy (sin.)	19 720	± 350	19 280
PS2446-4	KIA4760	6	N. pachy (sin.)	1100	± 60	660
PS2446-4	KIA1286	150	N. Pachy (sin.)	12 860	± 90	12 420
PS2446-4	KIA4761	180	Mixed forams	15 870	± 90	15 430
PS2446-4	KIA4762	357	Mixed forams	19 730	± 60	19 290
PS2446-4	KIA1285	420	Mixed forams	21 550	± 250	21 110
PS2446-4	KIA4763	520	Mixed forams	23 580	± 60	23 140
PS2447-4	KIA4768	174	Mixed forams	13 830	± 80	13 390

Schachtschabel, 1984). Compositional variations of organic matter (OM) were additionally inferred from the hydrogen index HI [mgHydroCarbon/gTOC] obtained from Rock-Eval pyrolysis (cf. Espitalié et al., 1984). In immature TOC-rich sediments, HI-values of <100 mgHC/gTOC are typical of TOM, whereas HI-values of 200–400 mgHC/gTOC are characteristic of organic matter with a significant amount of MOM (Tissot and Welte, 1984).

The carbonate content was calculated as $CaCO_3$ (%) = (TC − TOC) × 8.333 (for detailed method description see Stein, 1991). The dolomite content was measured by means of a Philips PW3020 diffractometer and determined using the Qualit software package, described in detail by Emmermann and Lauterjung (1990) and Vogt (1997).

Stable oxygen and carbon isotope measurements on the planktonic foraminifera *Neogloboquadrina pachyderma* sin. from the >63 μm fraction were performed by means of a Finnigan MAT 251 mass spectrometer (AWI, Bremerhaven). The results are expressed in the δ-notation (permille versus Vienna Pee Dee Belemnite (PDB)). The chosen samples for accelerator mass spectrometer (AMS) radiocarbon (^{14}C) dating were measured at the Leibniz Laboratory for Radiometric Dating and Stable Isotopic Research, University of Kiel, Germany (Table 1). The ^{14}C ages are $\delta^{13}C$-normalized and corrected for oceanic-reservoir effects by subtracting off 440 years (Mangerud and Gulliksen, 1975), however, we are aware that this correction is not invariable with time (Bard et al., 1994) and measured species (Forman and Polyak, 1997).

In order to estimate the amount of ice rafted debris (IRD), which is used to represent rates of iceberg calving (Elverhøi et al., 1995a) the coarse-grained detritus (>2 mm) was counted on X-ray radiographs in 1 cm intervals downcore expressed as No. >2 mm/10 ccm (Grobe, 1987).

3. Physiographic settings

The FVT, located between Svalbard and Franz Josef Land, forms the deepest and widest conduit from the northern Barents Sea into the Arctic Ocean (Fig. 1). In the PARASOUND profile, the trough intersects the continental slope at 410 m water depth and reaches a central depth of 512 m (81°01.4′N, 43°43.0′E). The continental slope north of the FVT shows, in the PARASOUND profile, an uneven to partly smooth relief and varies in slope gradient between 1.3 and 3.6°.

Today, the entire study area is located north of the oceanic polar front (Fig. 1) and hence strongly influenced by advecting water masses. The fresh surface water layer (<4–5°C, 31.0–34.2‰ salinity) is 5–30 m thick and caused by melting of the sea-ice cover (Loeng and Vinje 1979; Loeng, 1991), which varies substantially on seasonal and inter-annual timescales (cf. Vinje, 1976). A <5–15 m thick, stable transition layer separates the fresh surface water layer from the underlying Arctic Water layer (Gerdes and Schauer, 1997). The Arctic water originates from convection during sea-ice formation in fall and winter and is advected out of the Arctic Ocean into the

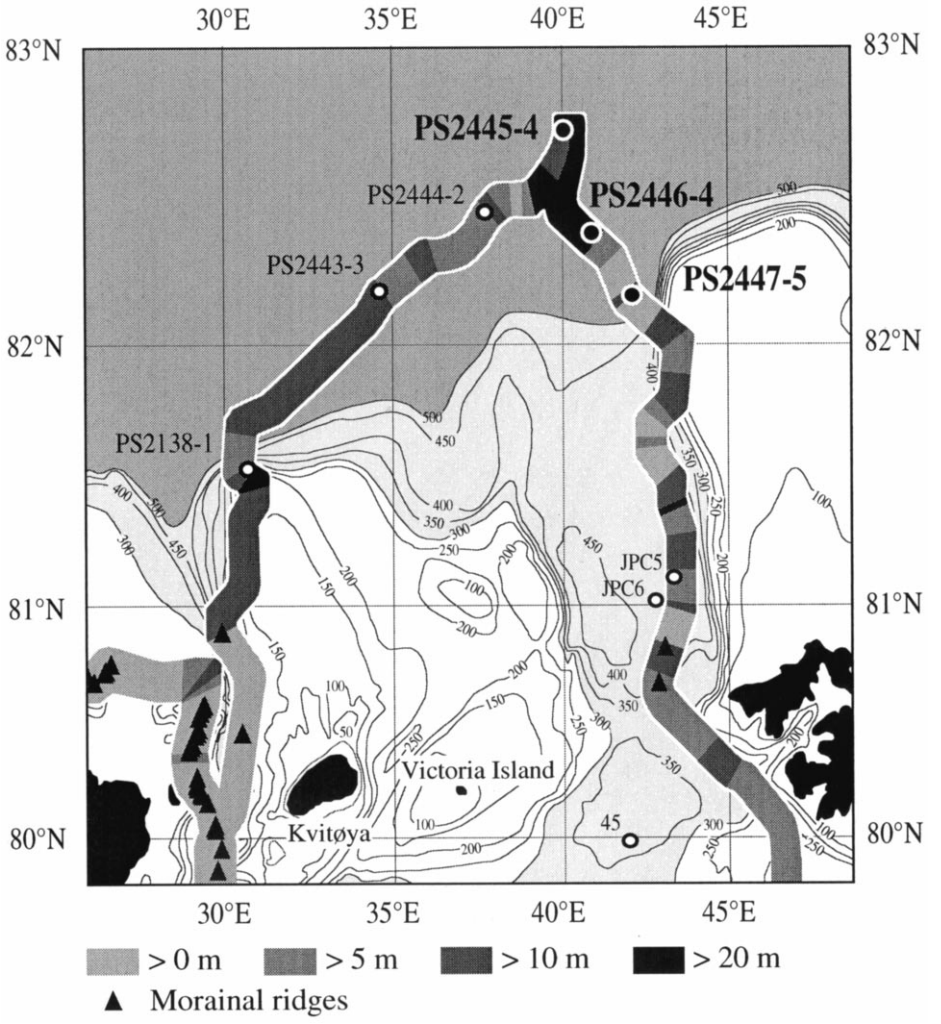

Fig. 2. Bathymetric map of the study area showing the minimum thickness of the Quaternary sediments, indicated by the maximum penetration of the PARASOUND system along the ship tracks.

Barents Sea by the ill-defined East Spitsbergen current (Fig. 1) (Mosby, 1938; Midttum and Loeng, 1987; Pfirman et al., 1994). The Arctic Water layer is typically found between 20 and 200 m and overlies the temperature and salinity maximum (<2.9°C, <35.0‰) of the northern Barents Atlantic-derived water masses (Fig. 1) between 200 and 500 m water (Mosby, 1938; Midttum and Loeng, 1987; Pfirman et al., 1994; Gerdes and Schauer, 1997). Below this Atlantic layer, down to several hundred meters water depth, lies a colder and less saline bottom water mass (Deep Arctic Ocean water, <0°C, >34.8‰) originating from the Norwegian-Greenland Sea and dense brine rejection during sea ice formation along the northern Barents Sea (Midttum, 1985; Rudels, 1986; Polyak and Solheim, 1994; Lubinski et al., 1996; Schauer et al., 1997).

4. Results

4.1. Seismostratigraphy

In the PARASOUND profiles (4 kHz) three seismic

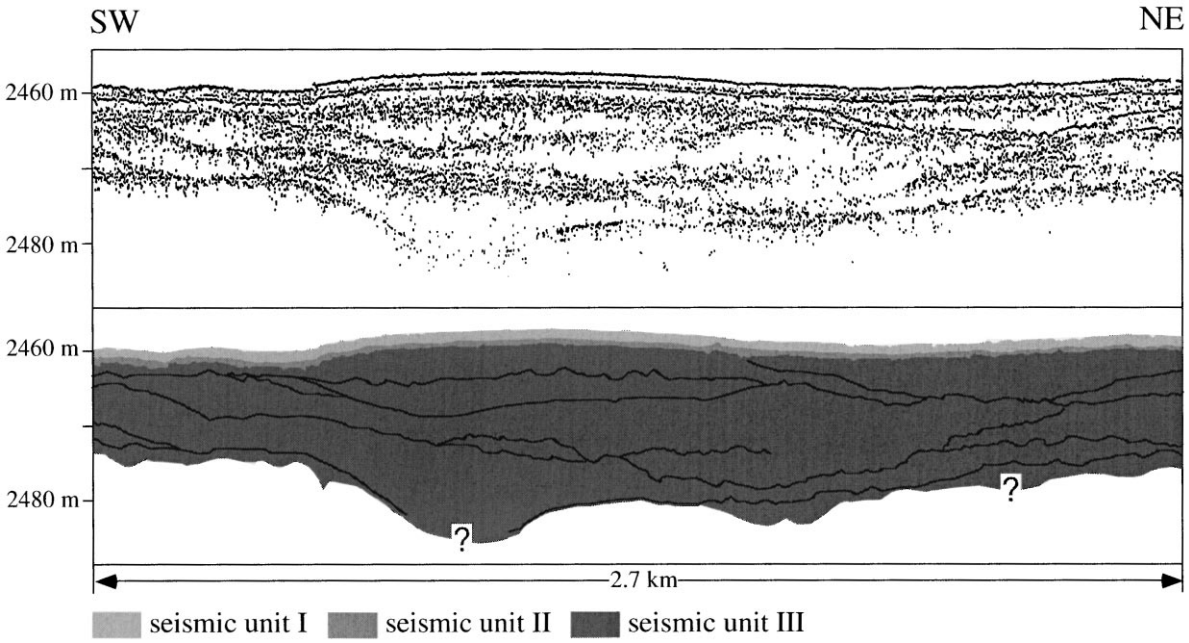

Fig. 3. PARASOUND profile showing truncating, stacked transparent lenses (for location see Fig. 1). The profile section was recorded while the ship remained on station during coring operation.

units were identified based on their internal reflection pattern, geometries and basal key seismic reflectors of mainly medium to high amplitude. Because the seismic signal is generally too weak to conclusively locate the Mesozoic sedimentary bedrock surface (Upper Regional Unconformity (URU) in the southern and western Barents Sea; Solheim and Kristoffersen, 1984), the mapped thicknesses of the Quaternary sediments represent only estimates of the minimum thickness (Fig. 2).

The uppermost seismic unit is acoustically transparent and drapes the variable topography of the underlying units (Figs. 3 and 4). The thickness of the upper unit varies between 0.5 and 2 m (Figs. 3 and 4).

The second seismic unit is on the continental shelf and west of core location PS2444 (Fig. 1) dominated by a continuous, prolonged to semi-prolonged reflector, limiting the acoustic penetration to 5–20 m. North of the FVT and in restricted PARASOUND profile sections west of Franz Josef Land (south of 81°31.1′N/43°10.7′E) and close to the shelf edge the acoustic penetration increases to 30 m (Fig. 2). In these PARASOUND profiles, the second seismic unit is of draping to infilling character, shows a subparallel layering or is acoustically transparent and varies in thickness between 1 and 5 m (Figs. 3 and 4). Northeast of Nordaustlandet, as far north as 80°53.6′N, 29°48.3′E (195 m water depth) (Fig. 2) the second seismic unit forms numerous ridges (Fig. 5) which are interpreted as moraines marking former ice margins. They are identified on the basis of their characteristic asymmetric shape and reveal a distinct to prolonged reflector. The morainal ridges reach up to several kilometers in width and a maximum height of 50 m. They are either exposed on the sea floor or conformably draped by the uppermost acoustic unit.

The third seismic unit was only identified in PARASOUND profiles from the continental slope east of core site PS2443 and from the FVT. On the continental slope north of the FVT, the third seismic unit is acoustically characterized by stacked, transparent lenses and layers (Figs. 3, 4 and 6). The seismically penetrated thickness of the third seismic unit varies generally around 20 m. Single layers and lenses reach up to 10 m in thickness, several kilometers in width and are separated by distinct to discontinuous reflectors or occasionally by layered sequences up to several meters thick. The lenses show irregular to

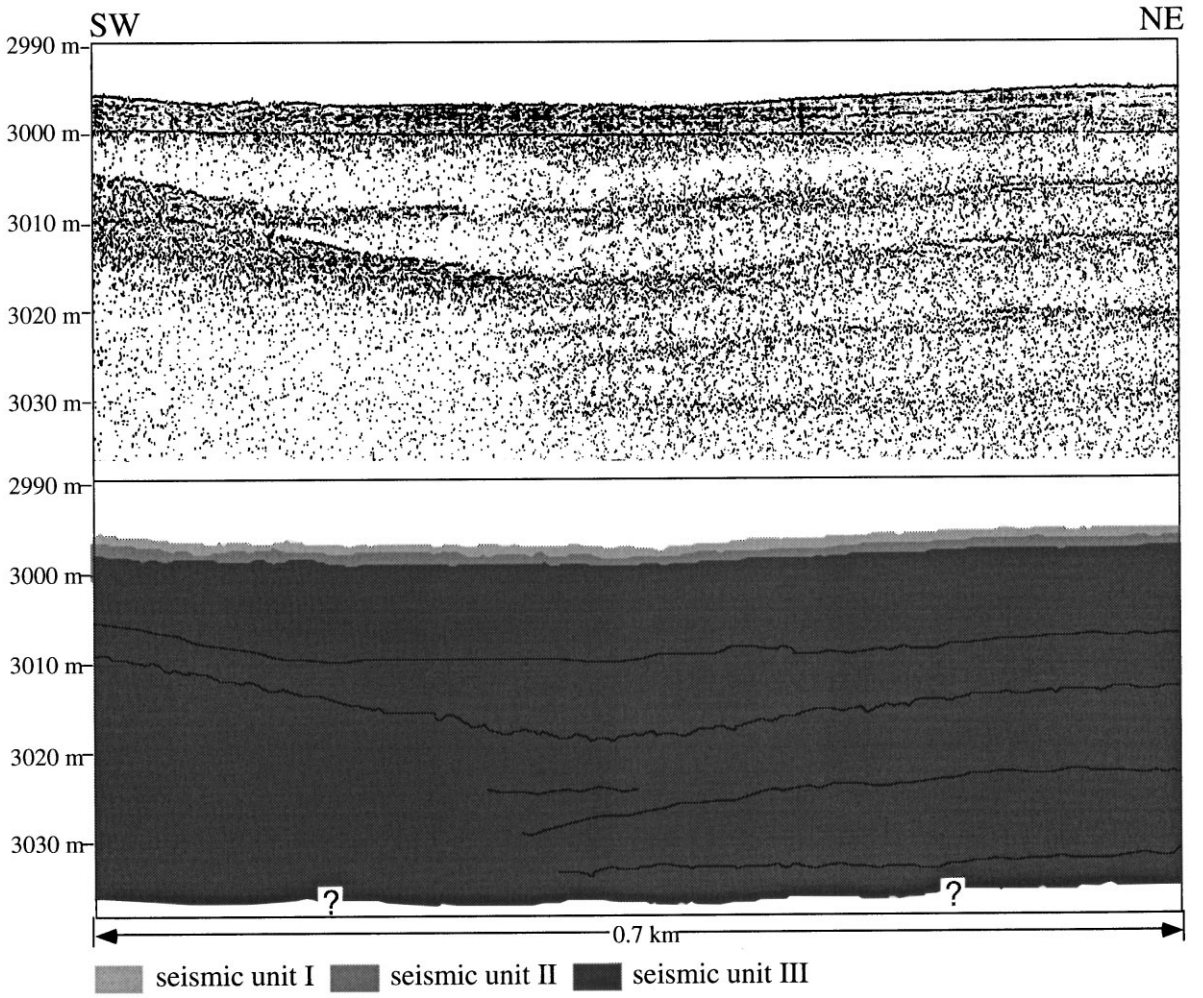

Fig. 4. PARASOUND profile showing transparent layers intercalated by transparent lenses (for location see Fig. 1). The profile section was recorded while the ship remained on station during coring operation.

convex shapes, wedge out and truncate the underlying sediments (Fig. 3). The layers are characterized by rather undisturbed, continuous thicknesses and mainly even to slightly wavy bases (Fig. 4). In places, the uppermost meters of the third seismic unit show either a intermitted layering, including core locations PS2446 and PS2447, or a prolonged surface echo, limiting the acoustic penetration <10 m.

In the FVT, the third seismic unit is dominated by the transparent facies. The basal reflector of the third seismic unit was only detected in limited profile sections south of 81°35′N. No internal reflectors were recorded from below this basal reflector, therefore the underlying seismic unit was described by Lubinski et al. (1996) as acoustic basement of unknown age. West of Franz Josef Land, as far north as 80°51.2′N, 43°11.0′E (460 m water depth), ridges interpreted as moraines were recorded. Because they are conformably draped by the uppermost transparent seismic unit and the subparallel layered second unit these moraines are assigned to the third seismic unit, unlike those northeast of Nordaustlandet.

4.2. Lithostratigraphy

The sedimentary record of the three studied

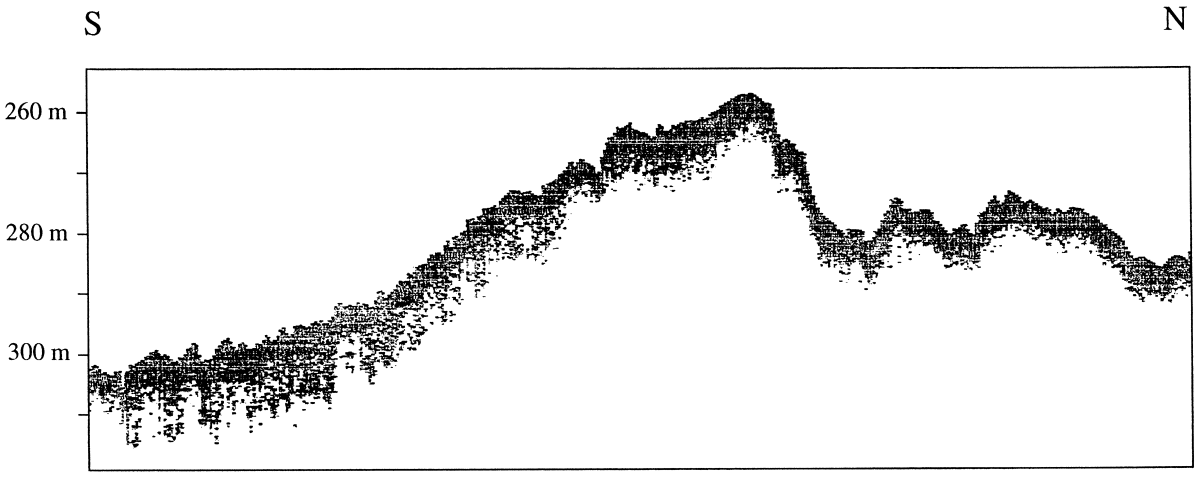

Fig. 5. PARASOUND profile recorded east of Nordaustlandet (for location see Fig. 1), showing a characteristic asymmetric cross section interpreted as morainal ridge. The ridge reveals a prolonged to semi-prolonged reflector and is exposed on the sea floor.

sediment cores (PS2445-4, PS2446-4 and PS2447-5) can be divided into five lithostratigraphic units on the basis of lithology, IRD content, sedimentary structures (Fig. 7). In addition, the subdivision is supported by geochemical features (Fig. 8).

Lithostratigraphic unit 1 represents, in all cores, the basal unit, consisting of a very dark olive gray, massive diamicton. The diamicton is matrix supported, poorly sorted and includes a high content of gravel, centimeter-sized stones and scattered mud clasts. The matrix is a sandy clayey silt. In core PS2447-5 the uppermost meters of the diamicton reveal a diffuse stratification. The TOC content ranges from 1.0 to 1.8 weight percent (%). C/N ratios vary between 20 and 30 and HI values are generally about 75 mgHC/gTOC. The upper massive diamicton in core PS2446-4 is lithologically and geochemically comparable to the basal diamictons, but shows an imbricated clast fabric and slightly normal grading.

Lithostratigraphic unit 2 consists of dark to olive gray, laminated silty clays, which are intercalated by gravel lenses and show a very low IRD proportion. Individual laminated silty clay layers show truncating, graded sandy bases. The laminated silty clays show a variable TOC content generally between 0.7 and 1.7 wt.%. C/N ratios range from 17 to 25 and the HI values from 50 to 75 mgHC/gTOC. The $CaCO_3$ content varies between 2 and 12 wt.%.

Lithostratigraphic unit 3 consists of dark to olive gray or grayish brown, bioturbated silty clays. Only sporadically a faintly lamination occurs. The bioturbated gray silty clays show TOC contents below 1 wt.% and C/N ratios between 12 and 17. The HI values vary between 25 and 75 mgHC/gTOC. Only the two basal HI values of the bioturbated gray silty clays intercalating the lower massive diamicton range between 125 and 150 mgHC/gTOC. The bioturbated gray silty clays show the highest $CaCO_3$ content of all units ranging between 6 and 15 wt.%. The IRD layer intercalating the bioturbated gray silty clays consists of small mud clasts.

Lithostratigraphic unit 4 consists of brown streaked, dark or olive gray, bioturbated, massive pebbly silty clays. Overall high contents of IRD with peak values consisting of mud clasts, scattered centimeter-sized cobbles and occasionally coal fragments (PS2446-4 and PS2447-4) characterize the massive pebbly silty clays. TOC contents vary from 0.3 to 1.6 wt.%, whereas the C/N ratios range from 11 to >30. The HI values are between 35 and 150 mgHC/gTOC. The $CaCO_3$ content varies considerably between 2 and 17 wt.%.

Lithostratigraphic unit 5 represents the uppermost core section including the surface sediments. It consists of a very dark brown to olive gray, bioturbated mud. The entire unit is rich in organic matter and only sporadically faintly laminated. The uppermost 20 cm of core PS2445-4 show a high abundance

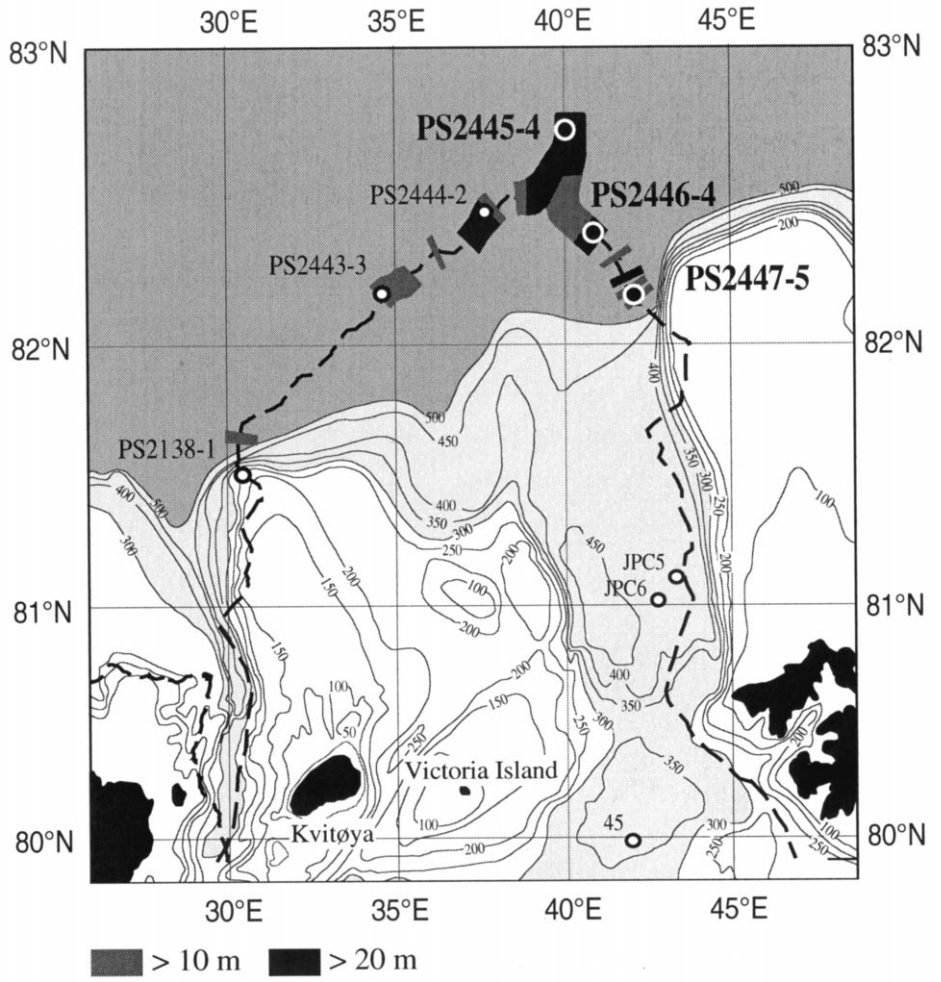

Fig. 6. Bathymetric map of the study area showing the distribution of the debris flow lobes identified in the PARASOUND profile.

of *Pyrgo* sp. (Fütterer, 1994). The IRD proportion is represented only by a few individual coarse sand grains. The TOC contents vary in core PS2446-4 from 0.8 to 1.4 wt.%, The C/N ratios range from 6 to 11, whereas the HI values vary between 40 and 85 mgHC/gTOC. The $CaCO_3$ content increases in core PS2446-4 from 1.5 at the base of the unit to 8 wt.% at the top.

4.3. Chronostratigraphy and sedimentation rates

The chronology of the sediment cores is based on nine AMS ^{14}C dates (Table 1). The dates show increasing ages with sediment depth. Furthermore, the stratigraphic framework of core PS2446-4 is supported by the stable oxygen and carbon isotope record of planktonic foraminifera *Neogloboquadrina pachyderma* sin. (Fig. 7).

Although the global oxygen isotope signal may be significantly compromised by local meltwater events, particularly in the lowermost part of core PS2446, the heaviest oxygen isotope values (up to 4.5‰) between 19.3 and 15.4 ^{14}C ka mark the marine isotope stage (MIS) 2. The final deposition of the lower massive diamicton on the lower and middle continental slope took place approximately 23 ^{14}C ka. This age was deduced from a sample of the bioturbated gray silty clay layer intercalating the massive diamicton in core

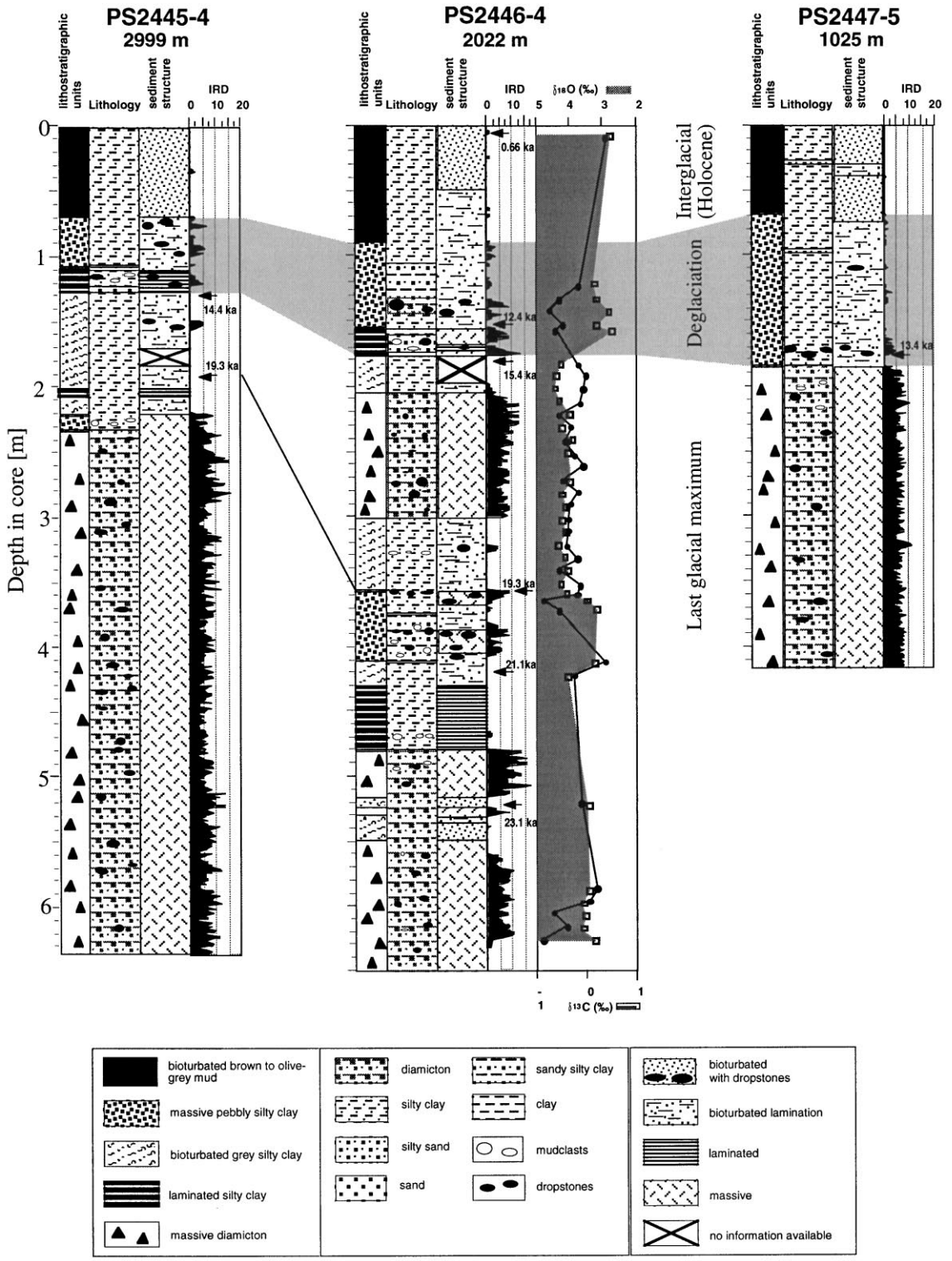
PS2445-4
2999 m
PS2446-4
2022 m
PS2447-5
1025 m
lithostratigraphic units
Lithology
sediment structure
IRD
0 10 20
δ18O (‰)
0 10 5 4 3 2
δ13C (‰)
- 1 0 1
Depth in core [m]
0
1
2
3
4
5
6
14.4 ka
19.3 ka
0.66 ka
12.4 ka
15.4 ka
19.3 ka
21.1ka
23.1 ka
13.4 ka
Interglacial (Holocene)
Deglaciation
Last glacial maximum
bioturbated brown to olive-grey mud
massive pebbly silty clay
bioturbated grey silty clay
laminated silty clay
massive diamicton
diamicton
silty clay
silty sand
sand
sandy silty clay
clay
mudclasts
dropstones
bioturbated with dropstones
bioturbated lamination
laminated
massive
no information available

PS2446-4 (Fig. 7). On the upper continental slope (PS2447-5) the deposition of the diamictons prevailed until about 13.4 ^{14}C ka. The deposition of the lower massive pebbly silty clay in core PS2446-4 occurred between 21.1 and 19.3 ^{14}C ka. The distinct decrease in δ^{18}O (1.3‰) after 15.4 ^{14}C ka marks the beginning of the transition from the last glacial period to the Holocene interglacial period (Termination I). Termination I is defined by two characteristic low-δ^{18}O spikes associated with distinct δ^{13}C minima values (−0.7‰), interpreted to reflect meltwater influx (cf. Stein et al., 1994), and a distinct IRD-input. The age of 12.4 ^{14}C ka marks the onset of MIS 1, which is characterized by relatively low δ^{18}O values and low δ^{13}C values.

The sedimentation rates were assumed by linear interpolation, whereby the thickness of the upper diamicton in core PS2446-4, interpreted as slump deposit (Fütterer, 1994), was subtracted for the sediment core. The linear sedimentation rates (LSRs) on the middle continental slope in front of the FVT vary between 9.1 and 49.3 cm/ky (Table 2). During the glacial period of MIS 2 the LSRs are higher (20.2–49.3 cm/ky) than during the Holocene interglacial period (<10 cm/ky). In general, the interpolated LSRs are comparable with the LSRs from the northern Barents Sea continental margin (Knies and Stein, 1998), the St. Anna Trough (Hald et al., 1999) and the Laptev Sea continental margin (Bauch et al., 1996; Spielhagen et al., 1996; Weiel, 1997; Stein et al., 1999).

5. Discussion

5.1. Last glacial maximum (LGM)

5.1.1. The glaciation of the Franz Victoria Trough

The PARASOUND profile (4 kHz) from the continental slope in front of the FVT reveals that the top of the transparent lenses and layers of the third seismic unit correspond with the lower diamictons in cores PS2445, PS2446 and PS2447. Transparent lenses were first interpreted by Damuth (1978) in 3.5 kHz records from the Bear Island and North Sea trough mouth fans, as debris flow deposits. In high latitudes, submarine fans constructed of stacked debris flow deposits and glacimarine diamictons reflect a periodic or continuous high sediment input from a fast-flowing glacier/ice sheet directly onto the upper continental slope, as described by e.g. Damuth (1978), Vorren et al. (1989), Vogt et al. (1993) and Laberg and Vorren (1996) for the Bear Island Trough or by Solheim et al. (1992) for the Isfjorden Fan on the Svalbard continental margin. The transparent layers represent according to Fütterer (1994) diamictons deposited at high sedimentation rates during the last or previous glaciations on the Barents Sea shelf. Therefore, we suggest that the thick sequence of debris flow lobes and diamicton layers were deposited when the grounding line of a SBIS reached the shelf break of the FVT (Fig. 9). The AMS ^{14}C age of 23.1 ka in the hemipelagic sequences intercalating the lower glacial diamicton in PS2446-4 approximates the advance of the grounding SBIS to the shelf break.

The sheet-like geometry, the absence of characteristic sediment lenses, the very limited acoustic penetration and the morainal ridges are strong evidences for interpreting the acoustically transparent, third seismic unit as basal till (cf. Lubinski et al., 1996). The identification of the key seismic reflector overlying the transparent third seismic unit in the PARASOUND profile of the FVT, supports the extent of the basal till to the shelf edge and thus the grounding of the northern SBIS in the entire FVT. The lack of morainal ridges in the PARASOUND profile in the northern FVT is a further indication that the grounding line of the SBIS reached the shelf edge (cf. Laberg and Vorren 1996). Continuously high TOC values (up to 1.5 wt.%) in association with C/N ratios >20 and low HI-values (<100 mgHC/gTOC) reveal the terrigenous character of the debris flow sediments and are indicative for a Svalbard/Barents Sea source area (Knies and Stein, 1998).

The restricted distribution of the gravity flow lobes in front of the FVT (Fig. 7) suggests that the trough acted as conduit for the fast-flowing ice stream as proposed by Elverhøi et al. (1995b) for the Isfjorden.

Fig. 7. Lithostratigraphic units, lithology, sedimentary structure and IRD content (numbers of detritus >2 mm in centimeter core intervals) of sediment cores PS2445-4, PS2446-4 and PS2447-5. Oxygen and carbon isotopes of core PS2446-4 are also displayed. AMS ^{14}C ages shown have been reservoir corrected using an age of 440 years (see Table 1).

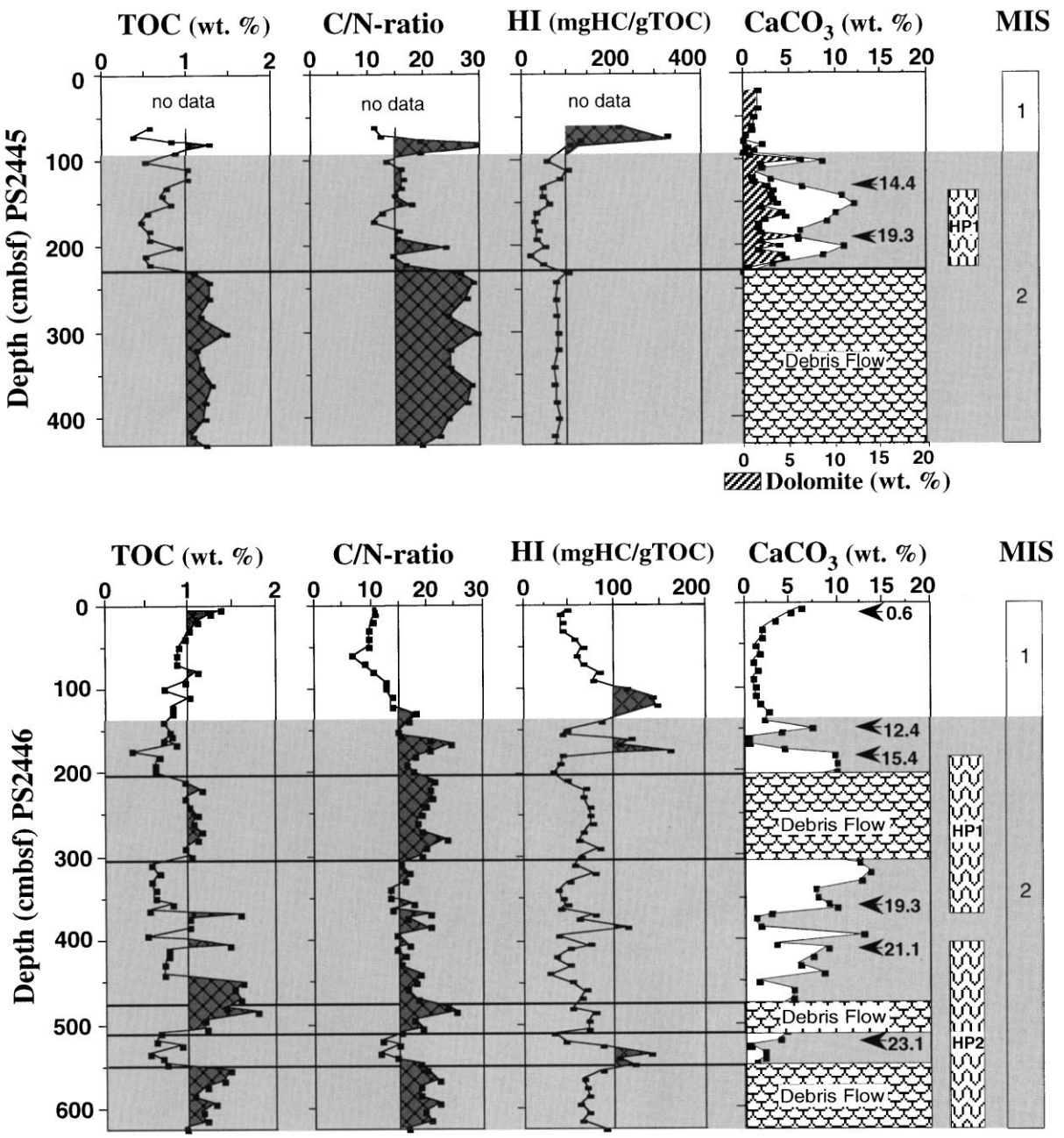

Fig. 8. Compilation of the total organic carbon, carbonate and dolomite content (all wt.%), C/N ratios and hydrogen index (HI) data versus core depth. Dolomite content in core PS2445-4 was published by Vogt (1997). Enrichment of carbonate rather than dolomite in core PS2445-4 indicates high amounts of planktic and benthic foraminifers. AMS ^{14}C datings and marine isotope stages (MIS) are shown on the right. HP1 and 2, high productive zones, are defined according to Dokken and Hald (1996).

Table 2
Sedimentation rates from core PS2446-4 in front of the Franz Victoria Trough based on AMS radiocarbon dates (Table 1)

Core no.	Sample interval (cm)	^{14}C years interval	Sidimentation rates (cm/1000 yr)
PS2445-4	131–191	14 400–19 280 ± 350	12.3
PS2446-4	0–6	0–660 ± 60	9.1
PS2446-4	0–150	0–12 420 ± 90	12.1
PS2446-4	150–180	12 420–15 430 ± 90	10.0
PS2446-4	180–357	15 430–19 290 ± 90	20.2
PS2446-4	357–420	19 290–21 110 ± 250	34.6
PS2446-4	420–520	21 110–23 140 ± 250	49.3

A canalization of the terminal ice zone in flow-parallel troughs descending 300–400 m below sea level is proposed by Boulton (1990), based on a simple numerical model. An increase in ice thickness by more than 200 m, compared to the adjacent shelf, will result in an enhanced flow and the tendency for an ice stream to develop (Boulton, 1990). An enhanced flow associated with an earlier glaciation, as suggested for the eastern Svalbard Islands by Elverhøi et al. (1995a), may help to explain the early advance of the northern SBIS to the shelf edge of FVT compared to western Svalbard. There, the SBIS reached the coast by ~22 ^{14}C ka (Andersen et al., 1996) and the maximum extension probably between 19.4 and 15 ^{14}C ka (cf. Elverhøi et al., 1995a; Landvik et al., 1998). In addition, a rather early extension of the northern SBIS into the FVT can be assumed from the vicinity to the hypothesized center of the ice sheet on Kong Karls Land, Svalbard (Forman et al., 1995), from there the ice flowed unhindered by bathymetric impediments to the FVT (Polyak and Solheim, 1994).

Furthermore, the distribution of the debris flow deposits in the PARASOUND profiles (Fig. 6) and the general lack of glacial fans off the northern Svalbard margin (Solheim et al., 1996) indicate that the continental margin west of the FVT is not directly influenced by a fast-flowing ice stream reaching the shelf edge. This is supported by Österholm (1990), who argued based on marine limits on northern Nordaustlandet (Fig. 1) at about 50 m a.s.l., that the SBIS extended only to the coast line during the Late Weichselian. However, a steep increase in bulk accumulation rates (up to 50 g/cm^2/ky) and highest rates of kaolinite in core PS2138-1 (Fig. 1), likely derived from glacially eroded bedrocks in the northern and central Barents Sea and thus, indicate ice-proximal conditions west of the FVT after 23 ^{14}C ka (cf. Knies et al., 2000). According to Dowdeswell et al. (1998), these ice-proximal conditions point to a more stable ice sheet margin west of the FVT. Because compared to a fast-flowing ice stream, the sediment delivery of a more stable ice sheet margin is greatly reduced, which may explain the absence of debris flow deposits.

5.1.2. Paleoceanographic conditions in front of the FVT during the LGM

Hebbeln et al. (1994) and Dokken and Hald (1996) suggested that relatively warm Atlantic Water from the North Atlantic Ocean advected into the Greenland–Iceland–Norwegian seas (GIN) in short term events between 27–22.5 and 19.5–14.5 ^{14}C ka and that the resulting seasonally ice-free waters acted as important regional moisture sources for the build-up of the SBIS. The bioturbated gray silty clay intercalating the lower massive diamicton in sediment core PS2446-4 exhibit bioturbation and an increased $CaCO_3$ contents (up to 5 wt.%), referring to high abundances of coccolithes as well as subpolar planktonic and benthic foraminifera (Andersen et al., 1996; Hebbeln and Wefer, 1997). In the study area, periods associated with increased bioproductivity point to seasonally overall ice-free water conditions caused by Atlantic water surface/subsurface advection and/or local polynyas caused by upwelling of relatively warm Atlantic subsurface water (Kellogg, 1980; Hebbeln and Wefer, 1991; Kohfeld et al., 1996). Therefore, we suggest that the bioturbated gray silty clay, approximated to 23.1 ^{14}C ka, indicates that the Atlantic Ocean Water inflow, which caused the high productive zone HP2 (29–22.5 ^{14}C ka; Dokken and

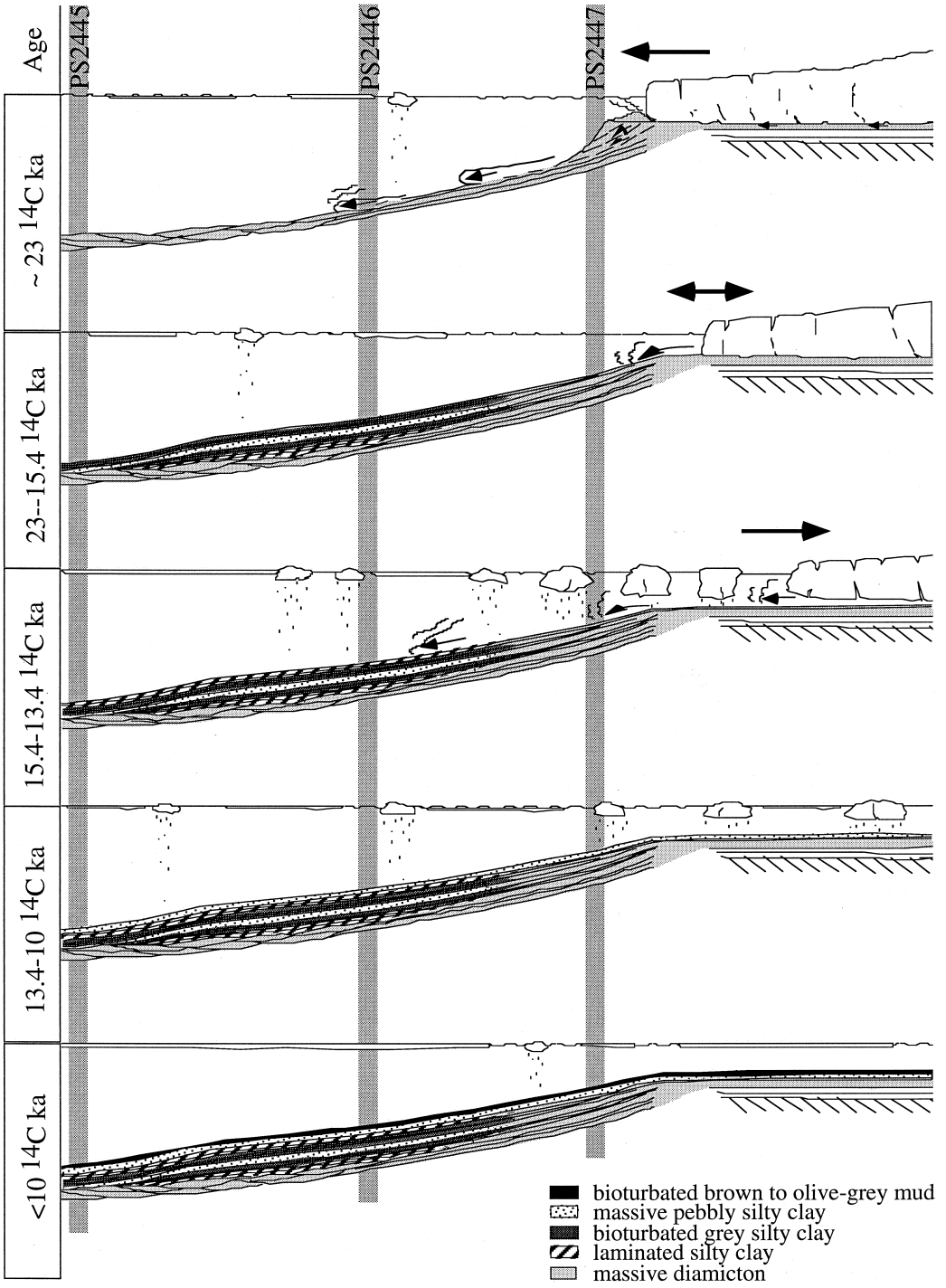

Fig. 9. Schematic models of the evolution of the northern Barents Sea continental margin during the Late Weichselian Glaciation showing the main processes on the shelf edge and the continental slope in relation to the behavior of the ice sheet at the shelfbreak.

Hald, 1996) along the western Svalbard continental margin, prevailed as far east as the FVT and acted as an important regional moisture source for the build-up of the SBIS onto the shelf edge (cf. Hebbeln et al., 1994; Knies et al., 1999).

The terrigenous character of the laminated sediments, directly overlying the lower debris flows deposits in core PS2446-4, is indicated by high TOC contents (up to 1.7 wt.%), C/N ratios >15 and low HI values (<75 mgHC/gTOC). The lack of bioturbation points to high sedimentation rates likely in relation with dense, turbid meltwater plumes draining the ice sheet located at the shelf edge directly on the continental margin (Fig. 9).

Severe bioturbation of the gray silty clay overlying the laminated sequence in association with $CaCO_3$ contents up to 9 wt.% indicates that seasonally ice-free water conditions prevailed until approximately 21 ^{14}C ka. These seasonally ice-free water conditions also confirmed by an enhanced supply of MOM indicated by low TOC contents (0.75 wt%), a drop in C/N ratios (<17) and slightly increasing HI values (up to 75 mgHC/gTOC), are likely related to a coastal polynya triggered by katabatic winds from the growing SBIS and an inflow of subsurface Atlantic water masses (cf. Knies et al., 1999).

The lower massive pebbly silty clay is characterized by a high IRD input indicating an increased calving rates of the SBIS between ~21 and 19.3 ^{14}C ka. The predominantly terrigenous origin of the sedimentary organic matter is documented by high C/N ratios (up to 20), variable TOC contents (0.5–1.5 wt%) and generally low HI values (<80 mgHC/gTOC). Because no further stacked gravity flow deposits occur on the lower continental slope north of the FVT, indicating a major grounding line displacement, we suggest that the low δ^{18}O values (3.5‰) and δ^{13}C minima values (−0.5‰), interpreted as meltwater signal, in association with significant IRD pulses refer to a temporary instability of the northern SBIS. This temporary instability coincides with the enormous discharge of icebergs to the North Atlantic (Heinrich Event H2: 21.6–19.4 ^{14}C ka) (Andrews and Tedesco, 1992; Bond et al., 1992; Broecker, 1994; Andrews et al., 1994).

The upper bioturbated gray silty clay in cores PS2445-4 and PS2446-4 is characterized by a high $CaCO_3$ (up to 7.5 wt.%) and a low TOC content (up to 0.8 wt%). Based on low dolomite contents in core PS2445-4, the increased $CaCO_3$ content is interpreted as biogenic calcite, although C/N-ratios around 15 and HI-values <100 mgHC/gTOC point to a predominantly terrigenous origin. The deposition of the upper bioturbated gray silty clay is approximated between 19.3 and 15.4 ^{14}C ka in core PS2446-4 and between 19.3 and 14.4 ^{14}C ka in core PS2445-4, respectively. Thus, the deposition coincides with the high productive zone HP1 (Dokken and Hald, 1996) and is therefore likely related to at least seasonally open water conditions caused by Atlantic water surface/subsurface advection to the Arctic Ocean (Hebbeln et al., 1994).

5.1.3. Deglaciation and Holocene

The initial disintegration of the northern SBIS (Termination I) marked in the cores from the middle and lower continental slope (PS2445-4 and PS2446-4) by a significant increase in IRD and the transition from heaviest δ^{18}O values (4.5‰) to a pronounced meltwater signal, displayed by δ^{18}O minina (3.2‰) and reduced δ^{13}C values (−0.57‰) (Fig. 7). The predominantly terrigenous origin of the sediments is supported by increasing TOC values (up to >1 wt%), high C/N ratios (up to 25) and very low carbonate contents (<5 wt%). This initial disintegration is approximated in core PS2446-4 to 15.4 ^{14}C ka. The first phase of disintegration until 12.4 ^{14}C ka is characterized by two distinct IRD peaks (Fig. 7). A decrease in IRD input during the first phase of deglaciation may be related to a stabilization of the ice sheet after the initial, huge input of icebergs. The subsequent cooling of the surface water after the first iceberg input promotes sea ice preservation and increases thereby the albedo. This in turn leads to a halt/readvance of the ice sheet and a reduced input of IRD. A cooling and temporary absence of open water conditions is supported by the contemporary deposition of laminated sediments. Their lack of bioturbation may indicate a poor ventilation of the water column (Phillips and Grantz, 1997). The occurrence of only one IRD event in the laminated sediments of core PS2445-4 on the lower continental slope signifies most likely that icebergs were blocked by permanent sea-ice and thus supports the transition from cold to warm conditions (Nam, 1997) (Fig. 9). If the single IRD peak in core PS2445-4 at 1.5 m represents a

short-time instability of the ice sheet or even correlates with the initial disintegration cannot be verified based on our datings and core data. An initial meltwater event at 15.4 ^{14}C ka is in good agreement with the first light-oxygen-isotope event in the eastern Arctic Ocean (Stein et al., 1994; Nørgaard-Pedersen et al., 1998), the Fram Strait (Jones and Keigwin, 1988), the western Svalbard margin (Jones and Keigwin, 1988; Hebbeln et al., 1994; Elverhøi et al., 1995a) and the northeastern Atlantic Ocean (Duplessy et al., 1981); it coincides with the cooling cycle predating the Heinrich event H1 (14.6–15.0 to 13.2–13.6 ^{14}C ka; McCabe and Clark, 1998). Therefore, we suggest that initial disintegration of the northern SBIS more likely reflects a climatic influence through a reduction in precipitation (McCabe and Clark, 1998) and/or a response to increased summer insolation rather than a response to the collapse of the Laurentide or other ice sheets in the northern hemisphere (cf. Dowdeswell et al., 1999). Furthermore, we suggest that the marine based nature of the SBIS, in addition with the morphology of the FVT, made it very susceptible to decoupling of the glacier bed caused by changes in relative sea-level at the specific tidewater margin (Jones and Keigwin, 1988; Andersen et al., 1996; Andrews, 1998). If the isostatical depression of the SBIS continued after the LGM it may have reached a critical level initiating the destruction of the ice sheet by marine downdraw through the FVT without external forcing, as described by Jones and Keigwin (1988) for the Bear Island and Storfjord troughs. The lack of the morainal ridges in the northern FVT supports a decoupling of the glacier bed during deglaciation. The change from massive to stratified diamicton on the middle and upper continental slope is interpreted as increased meltwater discharge of the grounded SBIS at the shelf edge of the FVT (e.g. Elverhøi et al., 1990, 1995b). Thus, the transition of the stratified diamicton to the massive pebbly silty clay approximated to ~13.4 ^{14}C ka (PS2447-5) may reflect the retreat of the northern SBIS from the shelf edge of the FVT (Fig. 9). This age is constrained in the northern FVT by the initial deposition of the ice proximal laminated clay at 13 ^{14}C ka overlying the diamicton, which is interpreted as a till (Polyak and Solheim, 1994; Lubinski et al., 1996). The prominent IRD pulses recorded in the upper massive pebbly silty clay indicate a discontinuous retreat of the SBIS. The onset of major IRD input in the upper massive pebbly silty clay is approximated in core PS2446 to ~12.4 ^{14}C ka. In core PS2445 the two major IRD events are dated based on linear interpolation to 12.3 and 10.7 ^{14}C ka, respectively. Therefore the two IRD pulses are in rather good correlation with distinct iceberg rafting events in the central FVT (Lubinski et al., 1996), on the Yermak Plateau (Vogt, 1997), the Saint Anna Trough (Polyak et al., 1997) and pulses of glacimarine sedimentation in the southeastern Barents Sea (Polyak et al., 1995). These ice rafting events are coeval with a period of increasing surface-water and air temperatures in the northern Atlantic region and accelerated eustatic sea-level rise, suggesting that the remaining retreat of the SBIS was paced by these factors (Polyak et al., 1995).

The bioturbated brown to olive-gray mud resembles in color, increased organic content, and very low IRD content sediments in the northern and central Barents Sea whose deposited began at ~10 ^{14}C ka (Elverhøi and Solheim, 1983; Elverhøi et al., 1989; Polyak and Solheim, 1994; Lubinski et al., 1996; Polyak et al., 1997). Apparently, the brown to olive-gray mud marks the end of the marine phase of deglaciation and points to the retreat of the SBIS to the present shoreline. Terrestrial evidences from Franz Josef Land and eastern Svalbard support this interpretation (Forman et al., 1995 and references therein). On basis of its thickness we suggest that the bioturbated brown to olive-gray mud, which in all cores represents the uppermost lithostratigraphic unit, corresponds to the uppermost, transparent seismic unit of draping character in the entire study area.

6. Summary and conclusions

Stacked, acoustic transparent lenses and layers in front of the FVT, interpreted as debris flow deposits and layers of glacimarine diamicton, indicate that large quantities of sediments were directly deposited by the northern SBIS onto the upper continental slope at approximately 23 ^{14}C ka. A grounding of the SBIS in the entire FVT is supported by the identification of the basal key seismic reflector overlying the acoustically transparent unit, interpreted as basal till near

the shelf break. The distribution of the gravity flow deposits on the continental slope suggests that the FVT acted as conduit and led to an enhanced flow of the northern SBIS. An enhanced flow in association with an earlier glaciation may help explaining the early advance of the northern SBIS to the shelf edge, compared to west Svalbard. The initial disintegration of the northern SBIS (Termination I) is indicated by an intensive increase of IRD to the continental slope at around 15.4 ^{14}C ka and a subsequent isotopically defined meltwater signal. This initial disintegration may reflect a climatic influence through a reduction of precipitation in association with the cooling cycle predating the Heinrich event H1, the decoupling of the glacier bed due to changes in relative sea level at the tidewater margin and/or a response to increased summer insolation. The grounding line retreat of the northern SBIS from the shelf edge of the FVT, indicated by a drastic change in sedimentary pattern on the upper continental slope is approximated to 13.4 ^{14}C ka. The stepwise deglaciation of the northern SBIS is documented by distinct IRD-pulses which appear to be contemporaneous with the onset of distinct pulses of IRD and glacimarine sedimentation in the adjacent areas between 13 and 9.4 ^{14}C ka.

Bioturbation indicated that seasonally open water conditions prevailed along the northern Barents Sea at least as far east as the FVT during the last glacial/interglacial cycle.

Acknowledgements

We are indebted to the captain and crew of RV *Polarstern* and our fellow scientists for their help in collecting the data. We thank the members of the Geology Section of the Alfred Wegener Institute for constructive discussions and Dr B. Diekmann, Dr C. Hass, Dr M. Pirrung, Dr R. Stein and Dr C. Vogt for correcting the manuscript. Special thanks goes to B. Kottke and A. Gierlichs for their help with the processing of the PARASOUND data. We thank the reviewers M. Hald and J.T. Andrews for valuable comments. This work was funded by the German Federal Ministry for Education, Research and Technology, BMBF-Forschungsverbund "ARKTIEF". This is contribution no. 1579 of the Alfred Wegener Institute.

References

Andersen, E.S., Dokken, T.M., Elverhøi, A., Solheim, A., Fossen, I., 1996. Late Quaternary sedimentation and glacial history of the western Svalbard continental margin. Mar. Geol. 133, 123–156.

Andrews, J.T., 1998. Abrupt changes (Heinrich events) in late Quaternary North Atlantic marine environments: a history and review of data and concepts. J. Quat. Sci. 13 (1), 3–16.

Andrews, J.T., Tedesco, K., 1992. Detrital carbonate-rich sediments, northwestern Labrador Sea: implications for ice-sheet dynamics and iceberg rafting (Heinrich) events in the North Atlantic. Geology 20, 1087–1090.

Andrews, J.T., Erlenkeuser, H., Tedesco, K., Aksu, A.E., Jull, A.J.T., 1994. Late Quaternary (stage 2 and 3) meltwater and Heinrich events, Northwestern Labrador Sea. Quat. Res. 41, 26–34.

Astakhov, V., 1992. The last glaciation of Siberia. Sver. Geol. Unders. Ser. C 81, 21–30.

Astakhov, V., 1998. The last ice sheet of the Kara Sea: terrestrial constraints on its age. Quat. Int. 45–46 (1), 19–28.

Bard, E., Arnold, M., Mangerud, J., Paterne, M., Labeyrie, L., Duprat, J., Melieres, M.-A., Sonstegaard, E., Duplessy, J.-C., 1994. The North Atlantic atmosphere-sea surface 14C gradient during the Younger Dryas climatic event. Earth Planet. Sci. Lett. 126, 275–287.

Bauch, H.A., Cremer, H., Erlenkeuser, H., Kassens, H., Kunz-Pirrung, M., 1996. Holocene paleoenvironmental evolution of the northern central Siberian shelf. Quaternary Environment of the Eurasian North (QUEEN), First Annual QUEEN Workshop, Strasbourg, France, Abstract Volume.

Bond, G., Heinrich, H., Broecker, W.S., Labeyrie, L., McManus, J., Andrews, J., Huon, S., Jantschik, R., Clasen, S., Simet, C., Tedesco, K., Klas, K., Bonani, G., Ivy, S., 1992. Evidence for massive discharge of icebergs into the North Atlantic ocean during the last glacial period. Nature 360, 245–249.

Boulton, G.S., 1990. Sedimentary and sea level changes during glacial cycles and their control on glacimarine facies architecture. In: Dowdeswell, J.A., Scourse, J.D. (Eds.). Glacimarine Environments; Processes and Sediments. Geological Society Special Publication, pp. 15–52.

Broecker, W.S., 1994. Massive iceberg discharge as triggers for global climate change. Nature 372, 421–424.

Damuth, J.E., 1975. Echo character of the western equatorial Atlantic floor and its relationship to the dispersal and distribution of terrigenous sediments. Mar. Geol. 18, 17–45.

Damuth, J.E., 1978. Echo character of the Norwegian-Greenland Sea: relationship to Quaternary sedimentation. Mar. Geol. 28, 1–36.

Damuth, J.E., 1980. Use of high-frequency (3.5–12 kHz) echograms in the study of near-bottom sedimentation processes in the deep-sea: a review. Mar. Geol. 38, 51–75.

Dokken, T.M., Hald, M., 1996. Rapid climatic shifts during isotope

stages 2–4 in the Polar North Atlantic. Geology 24 (7), 599–602.

Dowdeswell, J.A., Elverhøi, A., Spielhagen, R.F., 1998. Glacimarine sedimentary processes and facies on the Polar North Atlantic margins. Quat. Sci. Rev. 17, 243–272.

Dowdeswell, J.A., Elverhøi, A., Andrews, J.T., Hebbeln, D., 1999. Asynchronous deposition of ice-rafted layers in the Nordic seas and North Atlantic Ocean. Nature 400, 348–350.

Dunayev, N.N., Pavlidis, J.A., 1990. A model of the late Pleistocene glaciation of Eurasiatic arctic shelf. In: Kotlyakov, V.M., Sokolov, V.E. (Eds.). Arctic Research—Advances and Prospects (Vol. 2), Proceedings of the Conference of Arctic and Nordic Countries on Coordination of Research in the Arctic, Academy of Sciences of the USSR, Leningrad, December 1988. Academy of Sciences of the USSR, pp. 70–72.

Duplessy, J.C., Delibrias, G., Turon, J.L., Pujol, C., Duprat, J., 1981. Deglacial warming of the northeastern Atlantic Ocean: correlation with the paleoclimatic evolution of the European continent. Paleogeogr., Paleoclimatol., Paleoecol. 35, 121–144.

Elverhøi, A., Solheim, A., 1983. The Barents Sea ice sheet—a sedimentological discussion. Polar Res. 1, 23–42.

Elverhøi, A., Pfirman, S.L., Solheim, A., Larssen, B.B., 1989. Glaciomarine sedimentation in epicontinental seas exemplified by the northern Barents Sea. Mar. Geol. 85, 225–250.

Elverhøi, A., Nyland-Berg, M., Russwurm, L., Solheim, A., 1990. Late Weichselian ice recession in the Central Barents Sea. In: Bleil, U., Thiede, J. (Eds.). Geological History of the Polar Oceans: Arctic versus Antarctic, Kluwer Academic, Dordrecht, pp. 289–307.

Elverhøi, A., Fjeldskaar, W., Solheim, A., Nyland-Berg, M., Russwurm, L., 1993. The Barents Sea ice sheet—a model of its growth and decay during the Last Glacial Maximum. Quat. Sci. Rev. 12, 863–873.

Elverhøi, A., Andersen, E.S., Dokken, T.M., Hebbeln, D., Spielhagen, R., Svensen, J.I., Sørflaten, M., Rørnes, A., Hald, M., Forsberg, C.F., 1995a. The growth and decay of the Late Weichselian ice sheet in western Svalbard and adjacent areas based on provenance studies of marine sediments. Quat. Res. 44, 303–316.

Elverhøi, A., Svensen, J.I., Solheim, A., Andersen, E.S., Milliman, J., Mangerud, J., Hooke, R.L., 1995b. Late Quaternary sediment yield from the High Arctic Svalbard Area. J. Geol. 103, 1–17.

Emmermann, R., Lauterjung, J., 1990. Double X-ray analysis of cuttings and rock flour: a powerful tool for rapid and reliable determination of borehole lithostratigraphy. Scientific Drilling 1, 269–282.

Espitalié, J., Marquis, F., Barsony, I., 1984. Geochemical logging. In: Voorhess, K.J. (Ed.). Analytical Pyrolysis, Techniques and Applications, Butterworths, London, pp. 276–304.

Forman, S.L., Polyak, L., 1997. Radiocarbon content of pre-bomb marine mollusks and variations in the 14C reservoir age for coastal areas of the Barents and Kara seas, Russia. Geophys. Res. Lett. 24 (8), 885–888.

Forman, S.L., Lubinski, D., Miller, G.H., Snyder, J., Matishov, G., Korsun, S., Myslivets, V., 1995. Postglacial emergence and distribution of the late Weichselian ice-sheet loads in the northern Barents and Kara seas, Russia. Geology 23, 113–116.

Fütterer, D.K., 1994. The expedition ARCTIC'93, Leg ARK-IX/4 of RV "Polarstern" 1993. Rep. Polar Res. 149, 244.

Gataullin, V., Polyak, L., Epstein, O., Romanyuk, B., 1993. Glacigenic deposits of the Central Deep: a key to the Late Quaternary evolution of the eastern Barents Sea. Boreas 22, 47–58.

Gerdes, R., Schauer, U., 1997. Large-scale circulation and water mass distribution in the Arctic Ocean from model results and observations. J. Geophys. Res. 102, 8467–8483.

Grant, J.A., Schreiber, R., 1990. Modern swathe sounding and subbottom profiling technology for research applications: the Atlas Hydrosweep and Parasound systems. Mar. Geophys. Res. 12, 9–19.

Grobe, H., 1987. A simple method for the determination of ice-rafted debris in sediment cores. Polarforsch. 57 (3), 123–126.

Grosswald, M.G., 1980. Late Weichselian ice sheet of Northern Eurasia. Quat. Res. 13, 1–32.

Grosswald, M.G., 1990. Late Pleistocene ice sheet in the Soviet Arctic. In: Kotlyakov, V.M., Sokolov, V.E. (Eds.). Arctic Research—Advances and Prospects (Vol. 2), Proceedings of the Conference of Arctic and Nordic Countries on Coordination of Research in the Arctic, Academy of Sciences of the USSR, Leningrad, December 1988. Academy of Sciences of the USSR, pp. 70–72.

Grosswald, M.G., 1998. Late-Weichselian ice sheets in arctic and Pacific Siberia. Quat. Int. 45–46 (1), 3–18.

Hald, M., Kolstad, V., Polyak, L., Forman, S.L., Herlihy, F.A., Ivanov, G., Nescheretov, A., 1999. Late-glacial and Holocene paleoceanography and sedimentary environments in the St. Anna Trough, Eurasian Arctic Ocean margin. Paleogeogr., Paleoclimatol., Paleoecol. 146, 229–249.

Hebbeln, D., Wefer, G., 1991. Effect of ice coverage and ice-rafted material on sedimentation in the Fram Strait. Nature 350, 409–411.

Hebbeln, D., Wefer, G., 1997. Late Quaternary paleoceanography in the Fram Strait. Paleoceanography 12, 65–78.

Hebbeln, D., Dokken, T., Andersen, E.S., Hald, M., Elverhøi, A., 1994. Moisture supply for northern ice-sheet growth during the Last Glacial Maximum. Nature 370, 357–360.

Hughes, T., Denton, G.H., Grosswald, M.G., 1977. Was there a late-W rm Arctic Ice Sheet?. Nature 266, 596–602.

Jones, G.A., Keigwin, L.D., 1988. Evidence from the Fram Strait (78°N) for early deglaciation. Nature 336, 56–59.

Kellogg, T., 1980. Paleoclimatology and paleoceanography of the Norwegian-Greenland Sea: glacial-interglacial contrasts. Boreas 16, 267–292.

Knies, J., Stein, R., 1998. New aspects of organic carbon deposition and its paleoceanographic implications along the northern Barents Sea margin during the last 30,000 years. Paleoceanography 13 (4), 384–394.

Knies, J., Vogt, C., Stein, R., 1999. Late Quaternary growth and decay patterns of the Svalbard/Barents Sea ice sheet and paleoceanographic evolution along the northern Barents Sea margin. Geo-Mar. Lett. 18, 195–202.

Knies, J., Nowaczyk, N., Müller, C., Vogt, C., Stein, R., 2000. A multiproxy approach to reconstruct the environmental changes along the Eurasian continental margin during the last 150 000 years. Mar. Geol. 163 (1–4), 317–344.

Kohfeld, K.E., Fairbanks, R.G., Smith, S.L., Walsh, I.D., 1996. *Neogloboquadrina pachyderma* (sinistral coiling) as paleoceanographic tracers in the polar oceans: Evidence from Northeast Water Polynya plankton tows, sediment traps, and surface sediments samples. Paleoceanography 11 (6), 679–700.

Laberg, J.S., Vorren, T.O., 1996. The middle and late Pleistocene evolution of the Bear Island Trough Mouth Fan. Global Planet. Change 12, 309–330.

Lambeck, K., 1995. Constraints on the Late Weichselian ice sheet over the Barents Sea from observations of raised shorelines. Quat. Sci. Rev. 14, 1–16.

Lambeck, K., 1996. Limits on the areal extent of the Barents Sea ice sheet in Late Weichselian time. Global Planet. Change 12, 41–51.

Landvik, J.Y., Bondevik, S., Elverhøi, A., Fjeldskaar, W., Mangerud, J., Salvigsen, O., Siegert, M.J., Svendsen, J.-I., Vorren, T.O., 1998. The last glacial maximum of Svalbard and the Barents Sea area: ice sheet extent and configuration. Quat. Sci. Rev. 17, 43–75.

Loeng, H., 1991. Features of the physical oceanographic conditions of the Barents Sea. Polar Res. 10 (1), 5–18.

Loeng, H., Vinje, T., 1979. On the sea ice conditions in the Greenland and Barents Seas. In: Anon (Ed.). POAC 79th Proc. Fifth Int. Conf. Port and Ocean Engineering under Arctic Conditions. The Norwegian Institute of Technology, Trondheim, pp. 163–174.

Lubinski, D., Korsun, S., Polyak, L., Forman, S.L., Lehman, S.J., Herlihy, F.A., Miller, G.H., 1996. The last deglaciation of the Franz Victoria Trough, northern Barents Sea. Boreas 25, 89–100.

Mangerud, J., Gulliksen, S., 1975. Apparent radiocarbon ages of recent marine shells from Norway, Spitsbergen, and Arctic Canada. Quat. Res. 5, 263–273.

McCabe, A.M., Clark, P.U., 1998. Ice-sheet variability around the North Atlantic Ocean during the last glaciation. Nature 392, 373–377.

Midttum, L., 1985. Formation of dense bottom water in the Barents Sea. Deep-Sea Res. 32, 1233–1241.

Midttum, L., Loeng, H., 1987. Climatic variations in the Barents Sea. In: Loeng, H. (Ed.). The Effect of Oceanographic Conditions on Distribution and Population Dynamics of Commercial Fish Stocks in the Barents Sea, Proc. Third Soviet-Norwegian Symp., Murmansk, 26–28 May 1986. Institute of Marine Research, Bergen, pp. 13–27.

Mosby, H., 1938. Svalbard waters. Geofysiske Publikasjoner 12 (4), 1–85.

Nam, S.-I., 1997. Late Quaternary glacial history and paleoceanographic reconstructions along the East Greenland continental margin: evidence from high-resolution records of stable isotopes and ice-rafted debris. Rep. Polar Res. 241, 157.

Niessen, F., Kleiber, H.P., 1997. Marine sediment echosounding using PARASOUND. In: Stein, R., Fahl, K. (Eds.). Scientific Cruise Report of the Arctic Expedition ARK-XIII/2 of RV Polarstern. Reports on Polar Research, 255, pp. 99–105.

Nørgaard-Pedersen, N., Spielhagen, R.F., Thiede, J., Kassens, H., 1998. Central Arctic surface ocean environment during the past 80,000 years. Paleoceanography 13 (2), 193–204.

Österholm, H., 1990. The Late Weichselian glaciation and Holocene shore displacement on Prins Oscars Land Nordaustlandet, Svalbard. Geogr. Annal. 72A, 301–317.

Pfirman, S.L., Bauch, D., Gammelsrød, T., 1994. The northern Barents Sea: water mass distribution and modification. In: Johannessen, O.M., Muench, R.D., Overland, D.C. (Eds.). The Polar Oceans and their Role in Shaping the Global Environment. American Geophysical Union, Washington DC, USA, pp. 77–94.

Phillips, R.L., Grantz, A., 1997. Quaternary history of sea ice and paleoclimate in the Amerasia basin, Arctic Ocean, as recorded in the cyclical strata of Northwind Ridge. Geol. Soc. Am. Bull. 109, 1101–1115.

Polyak, L., Solheim, A., 1994. Late- and postglacial environment in the northern Barents Sea weat of Franz Josef Land. Polar Res. 13 (2), 197–207.

Polyak, L., Lehman, S.J., Gataullin, V., Jull, A.J.T., 1995. Two-step deglaciation of the southwestern Barents Sea. Geology 23, 567–571.

Polyak, L., Forman, S.L., Herlihy, F.A., Ivanov, G., Krinitsky, P., 1997. Late Weichselian deglacial history of the Svyataya (Saint) Anna Trough, northern Kara Sea, Arctic Russia. Mar. Geol. 143, 169–188.

Pratson, L.F., Laine, E.P., 1989. The relative importance of gravity-induced versus current-controlled sedimentation during the Quaternary along the mideast U.S. outer continental margin revealed by 3.5 kHz echo character. Mar. Geol. 89, 87–126.

Rudels, B., 1986. The theta–S relation in the northern seas. Implications for deep circulation. Polar Res. 4, 138–159.

Schauer, U., Muench, R.D., Rudels, B., Timokhov, L., 1997. Impact of eastern Arctic shelf waters on the Nansen Basin intermediate layers. J. Geophys. Res. 102 (C2), 3371–3382.

Scheffer, F., Schachtschabel, P., 1984. Lehrbuch der Bodenkunde, Enke-Verlag, Stuttgart (p. 442).

Siegert, M.J., Dowdeswell, J.A., 1995. Numerical modeling of the Late Weichselian Svalbard-Barents Sea Ice Sheet. Quat. Res. 43, 1–13.

Siegert, M.J., Dowdeswell, J.A., Melles, M., 1999. Late Weichselian glaciation of the Russian High Arctic. Quat. Res. 52 (3), 273–285.

Solheim, A., Forsberg, C.F., 1996. Norwegian Polar Institute's cruise to the northern margin of Svalbard and the Barents Sea 25/7–2/9, 1994: marine geology/geophysics and physical oceanography. Norsk Polarinstitutt.

Solheim, A., Kristoffersen, Y., 1984. Sediments above the upper regional unconformity: thickness, seismic stratigraphy and outline of the glacial history. Norsk Polarinst. Skrifter 179B, 26.

Solheim, A., Russwurm, L., Elverhøi, A., Nyland-Berg, M., 1990. Glacial flutes, a direct evidence for grounded glacier ice in the northern Barents Sea: implications for a pattern of deglaciation and late glacial sedimentation. In: Dowdeswell, J.A., Scourse, J.D. (Eds.). Glaciomarine Environments: Processes and Sediments, Geol. Soc. London Spec. Publ. 53, 18–23.

Solheim, A., Andersen, E.S., Elverhøi, A., Svendsen, J.I., Mangerud, J., 1992. Glacial history, sedimentation and processes on the Western Svalbard margin. Nordiske Geologiske Vintermøte, Reykjavik, 154p. (abstract).

Solheim, A., Leirdal, G., Nilsen, C.L., Elverhøi, A., Forsberg, C.F., 1996. Late Weichselian glacial extent and paleoenvironmental

evolution of the northern Svalbard-Barents Sea margin. Supplement to EOS, Transactions, AGU 77.

Spielhagen, R.F., Erlenkeuser, H., Heinemeier, J., 1996. Deglacial changes of freshwater export from the Laptev Sea to the Arctic Ocean. Quaternary Environment of the Eurasian North (QUEEN), First Annual QUEEN Workshop, Strasbourg, France, Abstract Volume.

Stein, R., 1991. Accumulation of Organic Carbon in Marine Sediments, Springer, Berlin.

Stein, R., Schubert, C., Vogt, C., Fütterer, D.K., 1994. Stable isotope stratigraphy, sedimentation rates, and salinity changes in the Latest Pleistocene to Holocene eastern central Arctic Ocean. Mar. Geol. 119, 333–355.

Stein, R., Fahl, K., Niessen, F., Siebold, M., 1999. Late Quaternary organic carbon and biomarker records from the Laptev Sea continental margin (Arctic Ocean): implications for organic carbon flux and composition. In: Kassens, H., Bauch, H.A., Dmitrenko, I., Eicken, H., Hubberten, H.-W., Melles, M., Thiede, J., Timokhov, L. (Eds.). Land–Ocean Systems in the Siberian Arctic: Dynamics and History, Springer, Berlin, pp. 635–656.

Svendsen, J.I., Astakov, V.I., Bolshiyanov, D.Yu., Demidov, I., Dowdeswell, J.A., Gataullin, V., Hjort, Ch., Hubberten, H.-W., Larsen, E., Mangerud, J., Melles, M., Möller, P., Saarnisto, M., Siegert, M.J., 1999. Maximum extent of the Eurasian ice sheet in the Barents and Kara Sea region during the Weichselian. Boreas 28, 234–242.

Tissot, B.P., Welte, D.H., 1984. Petroleum Formation and Occurrence. Springer, New York, p. 699.

Vinje, T.E., 1976. Sea Ice Conditions in the European Sector of the Marginal Seas of the Arctic, 1966–1975. Norsk Polarinstitutt Årbok, pp. 163–174.

Vinje, T.E., 1985. Drift, Composition, Morphology and Distribution of Sea Ice Fields in the Barents Sea. Norsk Polaristitutt Skrifter 179C, 26p.

Vogt, C., 1997. Regional and temporal variations of mineral assemblages in Arctic Ocean sediments as climatic indicator during glacial/interglacial changes. Rep. Polar Res. 251, 335.

Vogt, P.R., Crane, K., Sundvor, E., 1993. Glacigenic mudflows on the Bear Island Submarine Fan. EOS 74 (40), 449–453.

Vogt, P.R., Crane, K., Sundvor, E., 1994. Deep Pleistocene iceberg plowmarks on the Yermak Plateau: sidescan and 3.5 kHz evidence for thick calving ice fronts and a possible marine ice sheet in the Arctic Ocean. Geology 22, 403–406.

Vorren, T.O., Laberg, J.S., 1997. Trough mouth fans—palaeoclimate and ice-sheet monitors. Quat. Sci. Rev. 16, 865–881.

Vorren, T.O., Lebesbye, E., Andreassen, K., Larsen, K.-B., 1989. Glacigenic sediments on a passive continental margin as exemplified by the Barents Sea. Mar. Geol. 85, 251–272.

Weiel, D., 1997. Paläozeanographische Untersuchungen in der Vilkitsky Strasse und östlich von Severnaya Zemlya mit sedimentologischen und geophysikalischen Methoden. Ph.D. Thesis, Univ. Köln, 138pp.